JOURNAL OF MATERIALS SCIENCE **36** (2001) 1921–1929

Precipitation sequence in a SiC/Al-Mg_2Si alloy composite material

S. IKENO, K. MATSUDA, S. RENGAKUJI
Department of Materials Science and Engineering, Faculty of Engineering, Toyama University, 3190, Gofuku, Toyama-shi, Toyama, 930-8555, Japan
E-mail: ikeno@eng.toyama-u.ac.jp

Y. UETANI
Research Institute for Technology, Toyama Prefectural University, 5180, Kurokawa, Kosugi, Imizu-gun, Toyama, 939-0398, Japan

The precipitation sequence of an Al-1.0mass%Mg_2Si composite material having 8 vol.% SiC particles was investigated by Vickers micro hardness and specific electrical resistivity measurements, and by TEM observation. The formation of GP zones was suppressed in the composite material and its age-hardenability was reduced. Distribution of precipitates in the composite material was coarser and their size was larger than that in the Al-1.0mass%Mg_2Si alloy (base alloy). Some types of precipitates in the composite material were not similar to those found in the base alloy but were similar to those in an Al-1.0mass%Mg_2Si alloys with excess silicon (the excess Si alloy). Especially, the metastable phases in the composite material aged at 473 K belonged to the type-A, type-B and type-C precipitates, which are typical metastable phases in the excess Si alloy, instead of the β' phase that is a typical metastable phase in quasi-binary Al-Mg_2Si alloys. The dislocations had little effect on the aging process of this composite material, because of the small number of dislocations introduced by the quenching after solution treatment.

1. Introduction

Many studies had been performed on composite materials consisting of age-hardenable aluminum alloys and ceramics particles such as Al_2O_3 [1–3] or SiC [4–9]. In the composite material containing Al_2O_3 particles, age-hardenability was reduced due to the formation of spinel at the interface between the matrix and particles. The spinel was formed by the reaction between oxygen in the Al_2O_3 and the magnesium contained in the matrix alloys [10]. While, in the case of an Al-Cu-Mg alloy containing SiC particles [7], the aging behavior of the composite material showed a similar behavior to an Al-Cu-Mg alloy with Si additions [11]. Due to the decomposition of the SiO_2 layer, which formed at the surface of SiC particles, free silicon would be generated and then dissolved into the matrix [8]. In the composite material, the σ phase that precipitates in the Al-Cu-Mg-Si alloys was observed [7]. It was very difficult to clarify the effects of free silicon atoms on the aging process in the composite materials due to the coexistence of many kinds of precipitates (S′, β, σ phases etc.) and the inhomogeneous distribution of the each precipitate in the composite material.

Recently, the aging process of Al-Mg-Si alloys containing excess Si was clarified [12]. It was found that the crystal structure of the intermediate precipitates was completely changed from those in the balanced Al-Mg-Si alloy by the addition of a small amount of excess silicon. The Al-Mg-Si alloy system is very suitable as a matrix material for investigation of the effects of free silicon on the aging process of a composite material containing SiC particles, because quantitative data concerning the relationship between some types of metastable phases and excess silicon content has been reported in our recent work [12]. Detailed studies have not yet been performed concerning the crystal systems of precipitates formed during aging of SiC reinforced Al-Mg-Si alloy.

In this report, the aging process of composite material containing 8 vol% SiC particles in an Al-Mg-Si alloy was investigated to clarify the effects of free silicon on the aging behavior and also changes in the crystal structure of precipitates.

2. Experimental procedure

An Al-0.66mass%Mg-0.35mass%Si (almost 1.0mass% Mg_2Si) matrix alloy (referred to as base alloy hereafter) was made by melting 99.99 mass% pure aluminum, 99.9 mass% pure silicon and magnesium ingots, and then the molten alloy was cast into an iron mold. SiC particles of 1.1 μm diameter (Showa Denko Co. Ltd.) were used for the reinforcement. The preparation of the composite material was performed by

TABLE I Chemical compositions of alloys (mass%)

Alloys	Mg	Si	Fe	Cu	Ti	Mn	Cr	Zn	Mg2Si	Excess Si
Base alloy	0.62	0.35	<0.01	<0.01	<0.01	<0.01	<0.01	<0.01	0.96	<0.01
Excess Si alloy	0.62	0.73	<0.01	<0.01	<0.01	<0.01	<0.01	<0.01	0.98	0.37

the following techniques; the SiC particles were prepacked into a metal mold and the molten metals were injected under a limiting pressure around 700 MPa. The mold was rapidly cooled by use of a water jacket from the bottom. The volume fraction of SiC particles was about 8%. in the composite material. A base alloy with 0.4 mass% Si addition (referred to as excess Si alloy hereafter) was also prepared for comparison with the composite material. Table I shows the chemical compositions of these alloys. Billets having 30 mm diameter and 50 mm length were extruded at high temperature to bars with 7 mm diameter, then cut into thin disks to make specimens for micro-Vickers indentation studies and transmission electron microscope. The relative electrical resistivity was measured by a four-terminal method on the strip shaped specimen ($0.3 \times 4.0 \times 7.0$ mm). The base alloy, excess Si alloy and the composite material were solution-treated at 848 K for 3.6 ks, quenched into ice water, and then aged at 423, 473 and 523 K. Topcon EM002B type transmission electron microscopy (TEM) was used at 200 kV to observe the microstructures of the specimens.

3. Results

3.1. Aging at 423 K

Fig. 1a shows the changes in hardness of the base alloy, the excess Si alloy and the composite material aged at 423 K. The hardness value after the solution treatment of the composite material is higher than that of the excess Si alloy. The base alloy has the lowest value of the three. The hardness of the base alloy increased slightly in an early stage of aging. On the other hand, an abrupt increase in hardness is observed in the early stage of aging in excess Si alloys, then increased up to the peak value. The hardness in the composite material increased in the early stage of aging while the time to reach peak hardness, t_{max}, was shorter than those of the other two alloys. The increments of hardness between the as quenched and the peak condition (age-hardenability, ΔH) in the excess Si alloys is the highest, while that in the composite material is the lowest. Fig. 1b shows the results of the specific electrical resistivities. A constant value was observed in the early stage of aging in the base alloy and then the resistivity reduced slowly with increasing aging times. In the composite material, the increase of specific electrical resistivity could not be observed in the early stage of aging as was observed in the base alloy. On the other hand, the specific electrical resistivity increased in the excess Si alloy in an early stage of aging. This implies that GP zones formed in the first stage of aging at 423 K in the excess Si alloy [13]. Precipitation on the dislocations would be also seen in the matrix near a SiC particle of the composite material at an early stage of aging at 423 K, although that TEM picture was omitted. A small amount of the preferential precipitates on the dislocations was observed in this investigation, suggesting that inhomogeneous precipitation is not important for the aging behavior in the composite material.

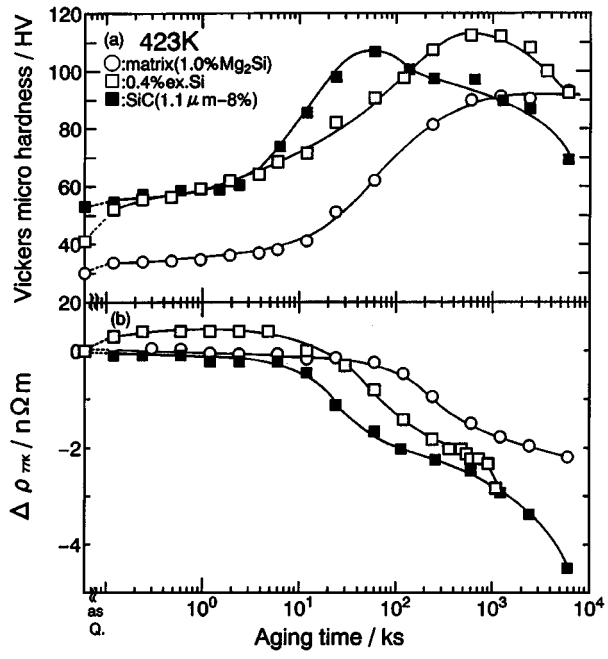

Figure 1 (a) Changes in the Vickers Micro Hardness of the base alloy, excess Si alloy and composite material aged at 423 K with aging time and (b) their specific electrical resistivities.

Fig. 2 shows TEM images of samples aged at 423 K up to t_{max}. Needle- or rod-shaped precipitates aligned parallel to ⟨100⟩ directions of the matrix in Fig. 2a were found in the base alloy aged at 423 K for 1200 ks. As shown in Fig. 2b, the finest precipitates were observed in the excess Si alloy at the peak condition. These fine precipitates account for the high hardness and age-hardenability found in this alloy. The peak hardness of the composite material was almost the same as that of the excess Si alloy but the age-hardening response was the lowest among the three alloys. The t_{max} of the composite material was greater than the other two alloys (see Fig. 1). The distribution of the precipitates in the composite materials (Fig. 2c) was coarser than those in other two alloys, so it is expected that the composite material would show the lowest hardening response among them. A number of characteristic precipitates (as judged by the HR images) which appeared with a relatively high frequency were found in the early stage of aging in the composite materials; an example is shown in Fig. 3a. This shows a precipitate in the composite material aged at 423 K; its longitudinal direction is

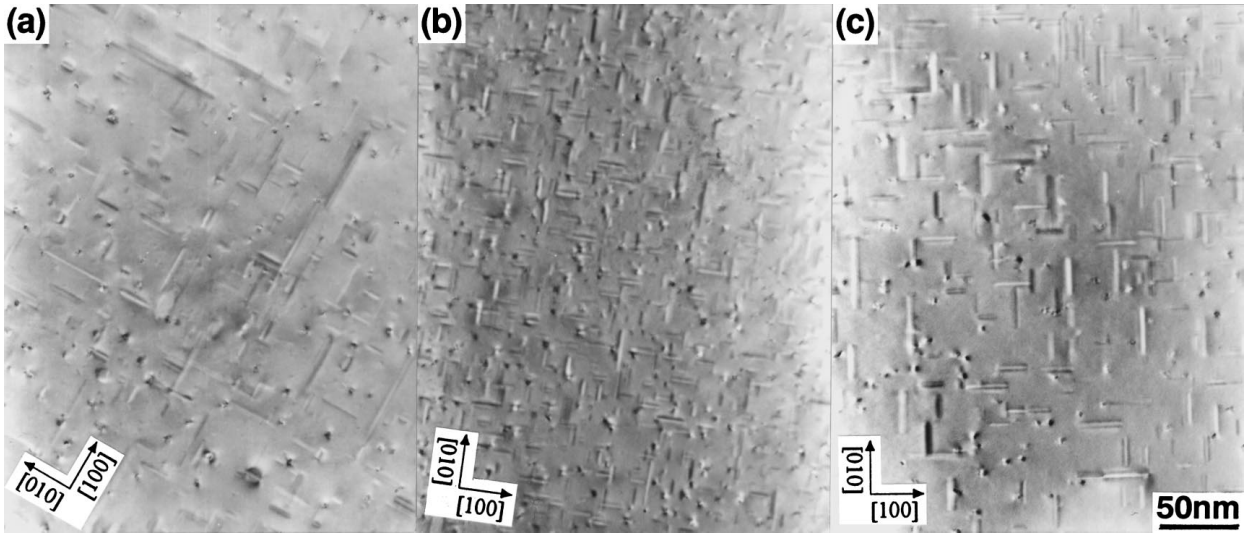

Figure 2 TEM images of specimens aged at 423 K up to their maximum hardness, t_{max}. (a) Base alloy, (b) excess Si alloy and (c) composite material.

parallel to this picture, so this is a cross section of the precipitate. The bright dots in this cross section do not show any periodic array corresponding to a particular crystal structure. This precipitate has been referred to as the 'random type' precipitate in our recent work on the precipitation sequence in Al-Mg-Si alloys [14]. Fig. 3b shows a precipitate that has a periodic array of bright dots. This type of precipitate is also referred as the 'parallelogram type' precipitate in our previous reports [15, 16]. A feature of this precipitate is that the length of the sides of the parallelogram range from 0.6–0.7 nm for its short side and 0.7–0.8 nm for its long side, while the included angle between the two sides has a range of 62–89 degrees. The two types of precipitates mentioned above do not have a rigid crystal structure and might be formed in the transition stage from the G.P. zone to metastable phases. Fig. 3c shows a precipitate having a spacing of bright dots of 0.67 and 0.77 nm and an included angle between the sides of 75 degree. In addition, an angle of 20 degrees was observed between the side of the parallelogram and ⟨100⟩ direction of the matrix. This type of precipitate is the β'' phase with a monoclinic crystal lattice [17]. Fig. 4 shows a summary of the changes in the relative frequency of each type of precipitate with aging time in the composite material. The random type precipitate is dominant in the early stage of aging. The parallelogram type precipitate accounts for less than 20 percent of the total in any aging stage. The β'' phase increases up to 70% with aging time. In the base alloy aged at 423 K, the parallelogram type precipitate was dominant while the β'' phase was somewhat observed, as shown in our recent work [18]. In the excess Si alloys, the parallelogram type precipitate was not observed and almost 100% β'' phase was found [19]. Although an Al-1.0mass%Mg_2Si alloy was used as the matrix alloy of the composite material, the types of precipitates were the same as those found in the excess Si alloy. Thus, it can be speculated that excess silicon element was formed by the decomposition of the SiC particles and dissolved into the matrix. The composition of the matrix shifted from a quasi-binary composition to the excess silicon side.

3.2. Aging at 473 K

As shown in Fig. 5a, at the higher aging temperature of 473 K, both the excess Si alloy and the composite material reached the maximum hardness in a shorter time than the base alloy. Furthermore, comparing with the response at 423 K, the time needed to reach maximum hardness is almost equal in the both alloys and the composite materials. The amount of hardening in the composite material at 473 K was again lower than those in the base alloy and in the excess Si alloy. In Fig. 5b, an increase of resistivity can be observed in the excess Si alloy alone.

Fig. 6 shows TEM images of all samples aged at 473 K up to their maximum hardness. Precipitates in the excess Si alloy are most densely distributed and this sample has the highest hardness. In the base alloy, a somewhat coarse and relatively large distribution of the precipitates is observed. In the composite material, a coarser distribution of the precipitates is observed than in either of the base alloys. The difference in size and distribution of precipitates in the samples are in good agreement with their maximum hardness values (Fig. 5a). The maximum hardness also provided by the parallelogram type of precipitate in the base alloy and by the β'' phase in the excess Si alloy. The changes in frequencies of the various types of precipitates in the composite material aged at 473 K with aging time are shown in Fig. 7. Three kinds of precipitates, namely the type-A, type-B and type-C precipitates begin to precipitate from a peak aged condition around 10 ks. In our recent reports, the type-A precipitate has a hexagonal crystal lattice with $a = 0.405$ and $c = 0.67$ nm. The type-B precipitate has an orthorhombic crystal lattice with $a = 0.683$, $b = 0.794$ and $c = 0.405$ nm and the type-C precipitate has a hexagonal crystal lattice with $a = 1.04$ and $c = 0.405$ nm [12]. In the base alloy aged at 423 or 473 K, only the β' phase precipitated and the three types of metastable phases were not observed in this work. Furthermore, our recent work has shown that three types of metastable phases precipitated while the β' phase did not form at these aging temperatures in the excess Si alloys [14]. Consequently, the precipitation sequence found for the composite material is

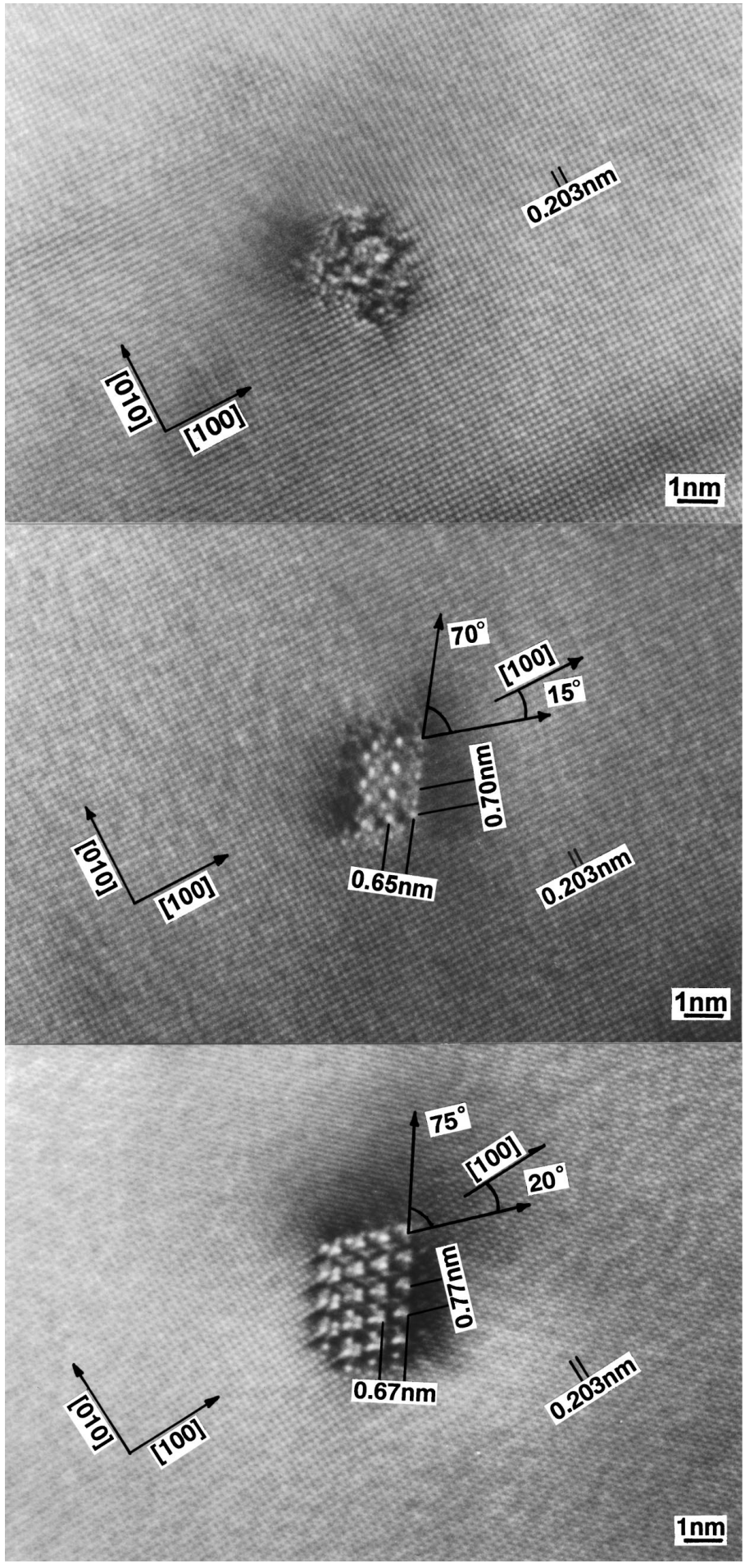

Figure 3 High-resolution TEM images of the cross section of needle-shaped precipitates taken from the composite material aged at 423 K for 240 ks. (a) The "random type" precipitate, (b) the parallelogram type precipitate and (c) the β''-phase.

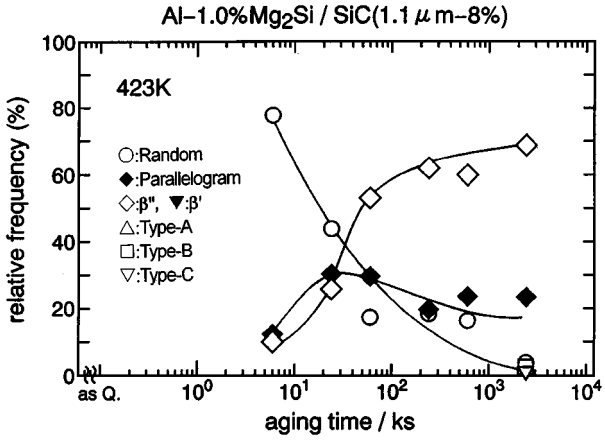

Figure 4 Changes in relative frequencies of each type of precipitate in the composite material aged at 423 K with aging time.

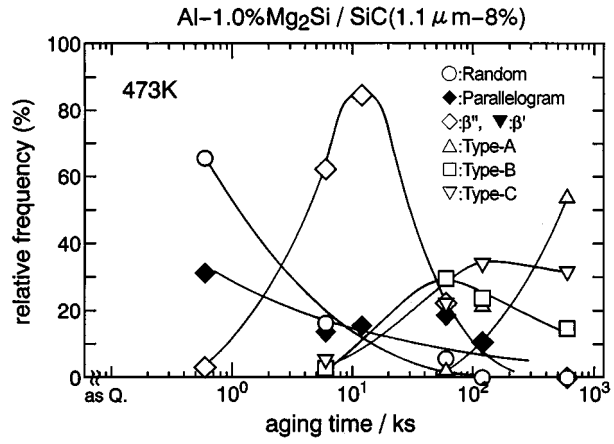

Figure 7 Changes in relative frequencies of each type of precipitate in the composite material aged at 473 K with aging time.

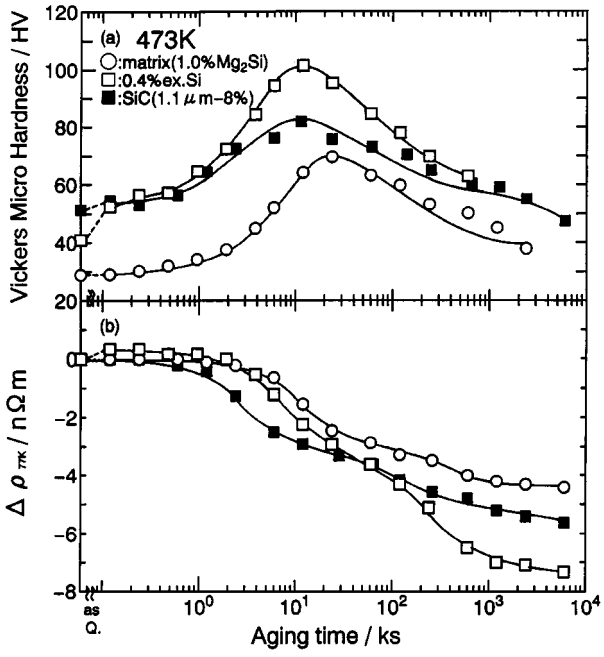

Figure 5 (a) Changes in the Vickers Micro Hardness of the base alloy, excess Si alloy and composite material aged at 473 K with aging time and (b) their specific electrical resistivities.

in good agreement with that observed in the excess Si alloys, although the quasi-binary base alloy was used as the matrix of the composite material.

3.3. Aging at 523 K

Fig. 8 shows age-hardening curves and specific electrical resistivities of the alloys and the composite material aged at 523 K. The t_{max} of the composite material and excess Si alloy occurred at a shorter time than that of the base alloy. The ΔH of the excess Si alloy was the highest among all the samples. Fig. 9 shows TEM images of samples aged at 523 K up to their peak-aged conditions. At low magnification, the excess Si alloy having the highest hardness had the finest distribution of the precipitates, while the precipitates in the base alloy were relatively coarser. The composite material had a coarser distribution and large spacing of precipitates. This tendency is in good agreement with the case of 473 K aging, namely, the highest hardness at the peak condition is provided by a denser and finer microstructure of precipitates in the matrix. The specific electrical resistivities of all the samples immediately decreased from their as-quenched condition at 523 K

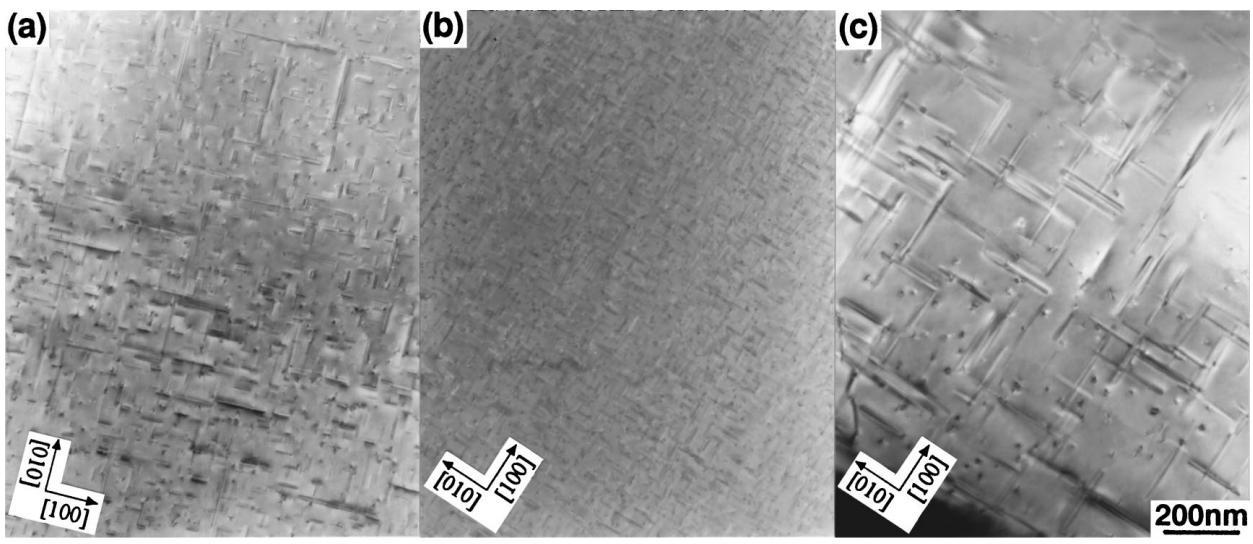

Figure 6 TEM images of specimens aged at 473 K up to their maximum hardness, t_{max}. (a) Base alloy, (b) excess Si alloy and (c) composite material.

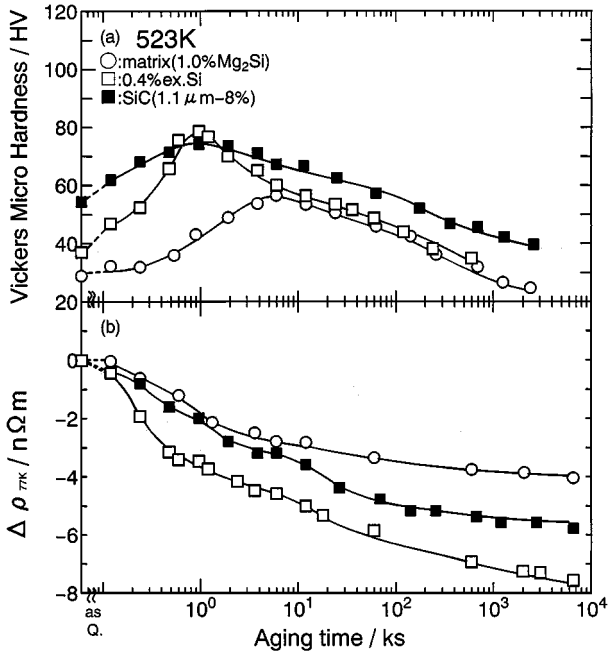

Figure 8 (a) Changes in the Vickers Micro Hardness of the base alloy, excess Si alloy and composite material aged at 523 K with aging time and (b) their specific electrical resistivities.

(compare Figs 1b, 5b and 8b) when the aging treatment was started. Therefore the formation of GP zones may not occur at this aging temperature. From the results of the TEM observation in our other reports [18, 19], the maximum hardness at 523 K can be obtained both for the base and excess Si alloys, when only the β' metastable phase is formed in the base alloy and only the β'' is precipitated in the excess Si alloy. As shown in Fig. 10, the type-B precipitate is formed in the composite material at the maximum hardness on its age-hardening curve. In Fig. 11a, a triangular shaped precipitate was observed in the overaged condition. This precipitate co-existed with the β (Mg_2Si)-phase. The electron diffraction pattern of Fig. 11b was identified as a ⟨111⟩ zone of silicon and the chemical analysis of Fig. 11c also indicated just silicon. The β phase is

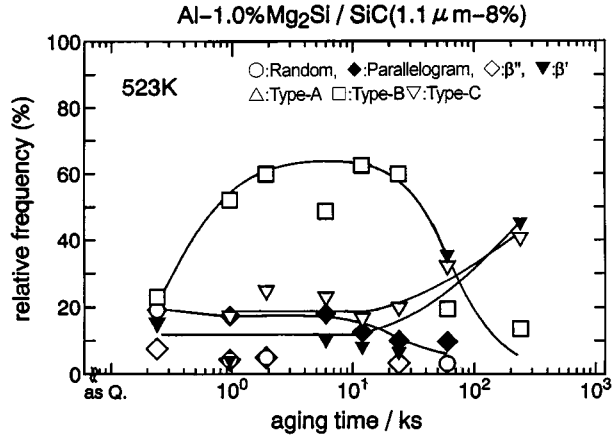

Figure 10 Changes in relative frequencies of each type of precipitate in the composite material aged at 523 K with aging time.

the only equilibrium phase in a stoichiometric, quasi-binary Al-Mg_2Si alloy, so it is expected that the equilibrium phase in the composite material is the β-phase, as found in the base alloy. According to our result, however, the Si phase also co-existed as the equilibrium phase in this composite material, as observed in the excess Si alloy. Thus the matrix of the composite material has an excess silicon contents.

4. Discussion

In our previous report [8], free silicon will be provided from the SiO_2 layer formed at the surface of SiC particles by a reaction between the oxide layer and the matrix, with the free silicon dissolving in the matrix. Finally, the matrix of the composite material will contain excess Si. The thickness of the SiO_2 layer on SiC particles to provide the 0.4 mass% of free silicon can be calculated to be 24 nm, assuming that all the SiC particles used in this investigation are spherical in shape and their mean radius is 1.1 μm. This thickness is reasonable, because 50 nm thickness of SiO_2 layer on the surface of 13 μm SiC particles diameter has been previously reported [9].

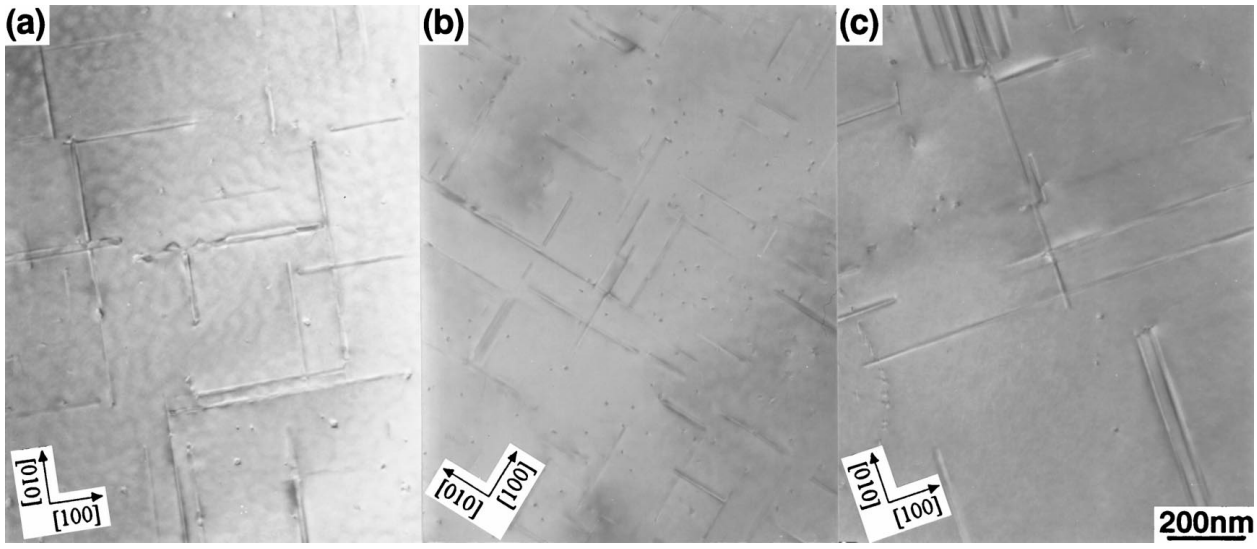

Figure 9 TEM images of specimens aged at 473 K up to their maximum hardness, t_{max}. (a) Base alloy, (b) excess Si alloy and (c) composite material.

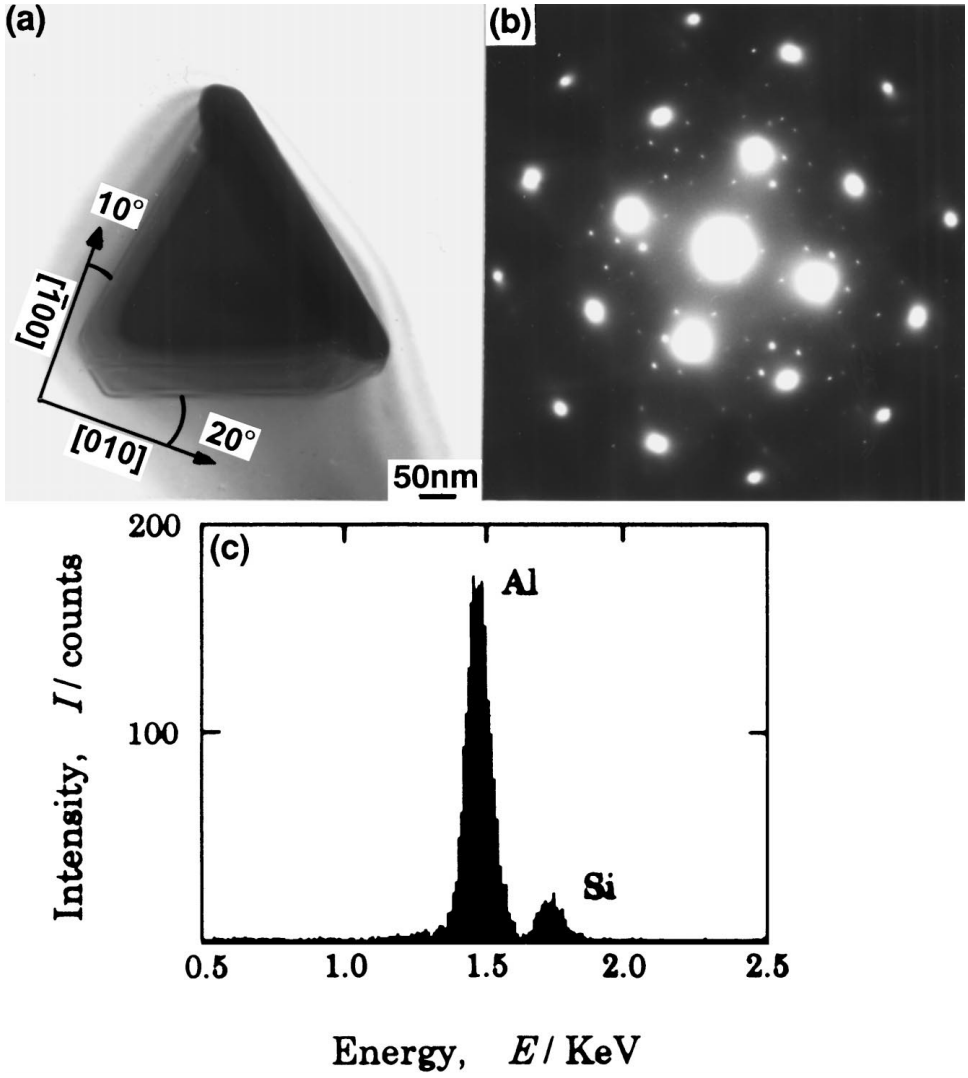

Figure 11 (a) A TEM image of a Si particle in the composite material aged at 523 K for 1200 ks, (b) its selected area diffraction pattern and (c) its EDS profile.

The acceleration of the aging process in SiC particle-dispersed Al-Mg-Si alloy composite materials may be caused by the preferential formation of the β' phase on the dislocations [20–22]. In this work, however, it is obvious that the composite material has the same types of precipitate as those in the excess Si alloy rather than the typical β' phase found in the base alloy.

At a relatively low aging temperature such as 423 K, the formation of GP zones may be retarded by the reduction of the excess vacancy concentration in the matrix due to the absorption of vacancies into the interfaces between particles and the matrix, or at dislocations during quenching. As a consequence of the depression of the GP zone and increased silicon content, the precipitation of metastable phases such as the type-A, type-B and type-C precipitates is accelerated in the composite material. On the other hand, at a higher aging temperature of 523 K, in spite of the depression of GP zones in the base alloy and the composite material, the acceleration of the aging process in the composite material is caused by the precipitation of different types of metastable phases in the matrix. The type-B precipitate was observed at the peak aging condition of the composite material. The type-B precipitate has a different crystal structure from the β' phase. The type-B precipitate has an orthorhombic crystal lattice and contains aluminum, magnesium and silicon in the ratio of 4 : 5 : 2 [23], while the β' phase has a hexagonal lattice and contains magnesium and silicon [24]. Fig. 12 shows HRTEM images of precipitates in the composite materials aged at 523 K. the β' phase or the type-C precipitate were often observed attached to the B type precipitates, and the regions of β' and type-C increased with progressing of aging time. So the type-B precipitate provides the nucleation site or acts as nuclei for the β' phase and type-C precipitate. It has been already clarified that the type-C precipitate is the predominant precipitate in the precipitation sequence of deformed excess Si alloys containing a high density of dislocations, although the type-B precipitate was much suppressed in the same sample [25]. So the acceleration of the precipitation sequence due to the preferential precipitation of the β' phase on dislocations introduced by quenching after solid solution treatment can not explain the present results, because the β' phase has a different crystal structure from the type-B precipitate [23, 24].

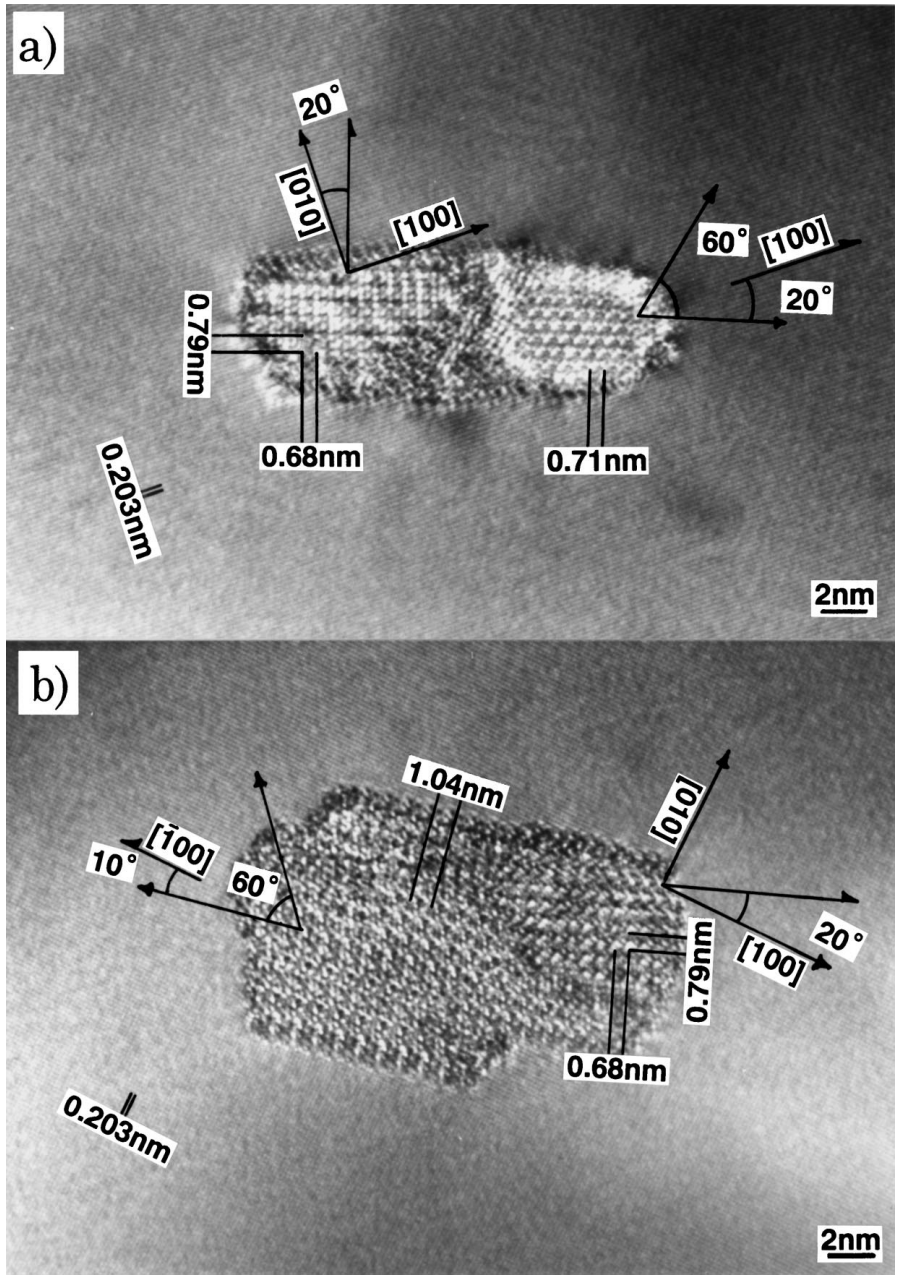

Figure 12 HRTEM images of precipitates in the composite material aged at 523 K. (a) Aged for 12 ks and (b) for 1.92 ks. In Fig. 12a, the β' phase (right region) is joined to the Type-B precipitate (left region), while type-C precipitate (left region) is joined to the type-B precipitate (right region) in Fig. 12b.

5. Conclusions

The precipitation sequence of the composite material having 8 vol.% SiC particles was investigated by micro Vickers hardness and specific electrical resistivity measurements, and by TEM observation. Obtained results are summarized as follows:

1. The formation of GP zones was suppressed in the SiC particle dispersed composite material and the aging hardening effect was reduced. The distribution and size of precipitates in the composite material were coarser than those in the base alloy.

2. Preferential precipitation on dislocations induced by the quenching after solution treatment was observed, but this was not the main precipitation reaction. The types of precipitates found in the composite material were not the same as those in the base alloy, but were similar to those found in the excess Si alloys, The metastable phases in the composite material aged at 473 K were type-A, type-B and type-C precipitates, typical of the excess Si alloy, instead of the β' phase. The matrix of the composite material contained a higher silicon content than the base alloy due to the free silicon liberated by reaction of the oxide on the SiC particles, although the base alloy was used as the matrix of the composite material.

3. At the higher aging temperature of 523 K, the type-B phase particles were precipitated at the maximum hardness point, while the type-C, which preferentially precipitated on the dislocations, were only present in a small amount. The effects of the dislocations on the aging process are minimal because of the low density of dislocations introduced by quenching after solution treatment.

References

1. D. YU and T. CHANDRA, *Mater. Trans. JIM* **12** (1993) 1184.
2. S. IKENO, K. KAWASHIMA, K. MATSUDA, H. ANADA and S. TADA, *J. Japan Inst. Light Met.* **40** (1990) 501.
3. S. IKENO, K. KAWASHIMA, K. MATSUDA, Y. UETANI, H. ANADA and S. TADA, *J. Society of Mater. Sci. Japan* **41** (1992) 1526.
4. S. I. HONG, G. T. GRAY III and J. J. LEWANDOWSKI, *Acta Metall.* **41** (1993) 2337.
5. M. P. THOMAS and J. E. KING, *J. Mater. Sci.* **29** (1994) 5272.
6. G. M. JANOWSKI and B. J. PLETKA, *Met. Mater. Trans. A* **26A** (1995) 3027.
7. S. IKENO, K. FURUTA, T. TERAKI, K. MATSUDA, H. ANADA and Y. UETANI, *J. Japan Inst. Light Met.* **46** (1996) 9.
8. N. WANG, Z. WANG and G. C. WEATHERLY, *Met. Trans. A* **23A** (1992) 1423.
9. H. RIBS, M. SUERY, G. L'ESPERANCE and J. G. LEGOUX, *ibid.* **21A** (1990) 2489.
10. K. SUGAMATA, G. SASAKI, T. FUJITA and N. SUZUKI, *J. Japan Inst. Light Met.* **41** (1991) 297.
11. R. D. SCUELLER, F. E. WAWNER and A. K. SACHDEV, *J. Mater. Sci.* **29** (1994) 239.
12. K. MATSUDA, Y. SAKAGUCHI, Y. MIYATA, Y. UETANI, T. SATO, A. KAMIO and S. IKENO, *ibid.* **35** (2000) 179.
13. C. PANSERI and T. FEDERIGH, *J. Inst. Met.* **94** (1966) 99.
14. K. MATSUDA, T. KAWABATA, T. NAOI, Y. UETANI, S. RENGAKUJI, T. SATO, A. KAMIO and S. IKENO, *J. Japan Inst. Met.* **62** (1998) 827.
15. K. MATSUDA, T. YOSHIDA, T. WADA, M. YOSHIDA, Y. UETANI, T. SATO, A. KAMIO and S. IKENO, *ibid.* **62** (1998) 718.
16. K. MATSUDA, T. YOSHIDA, H. GAMADA, K. FUJII, Y. UETANI, T. SATO, A. KAMIO and S. IKENO, *ibid.* **62** (1998) 133.
17. K. MATSUDA, T. NAOI, K. FUJII, Y. UETANI, S. RENGAKUJI, T. SATO, A. KAMIO and S. IKENO, *Mater. Sci. Eng.* **A262** (1998) 232.
18. K. MATSUDA, H. GAMADA, K. FUJII, T. YOSHIDA, T. SATO, A. KAMIO and S. IKENO, *J. Japan Inst. Light Met.* **47** (1997) 493.
19. K. MATSUDA, S. IKENO, T. SATO and A. KAMIO, in Proc. Thermec' 97, edited by T. Chandra and T. Sakai (TMS, 1997) p. 1027.
20. K. MATSUDA, H. GAMADA, Y. UETANI, S. RENGAKUJI, F. SHINAGAWA and S. IKENO, *J. Japan Inst. Light Met.* **48** (1998) 471.
21. H. TODA, T. KOBAYASHI and M. NIINOMI, *ibid.* **56** (1992) 1303.
22. H. J. RACK and R. W. KRENZER, *Met. Trans. A* **8A** (1977) 335.
23. K. MATSUDA, S. IKENO, T. SATO and A. KAMIO, *Scripta Mater.* **34** (1996) 1797.
24. K. MATSUDA, S. IKENO and S. TADA, *J. Japan Inst. Met.* **57** (1993) 1107.
25. K. MATSUDA, S. SHIMIZU, H. GAMADA, Y. UETANI, F. SHINAGAWA and S. IKENO, *J. Society of Mater. Sci. Japan* **48** (1999) 10.

Received 14 March
and accepted 15 September 2000